Atmos. Chem. Phys. Discuss., 13, 16457–16494, 2013
www.atmos-chem-phys-discuss.net/13/16457/2013/
doi:10.5194/acpd-13-16457-2013

Atmospheric Chemistry and Physics Discussions

Development of a source oriented version of the WRF/Chem model and its application to the California Regional $PM_{10}/PM_{2.5}$ Air Quality Study

H. Zhang[1], S. P. DeNero[1], D. K. Joe[1], H.-H. Lee[2], S.-H. Chen[2], J. Michalakes[3], and M. J. Kleeman[1]

[1]Department of Civil and Environmental Engineering, University of California, Davis. One Shields Avenue, Davis CA, USA
[2]Department of Land, Air, and Water Resources, University of California, Davis. One Shields Avenue, Davis CA, USA
[3]National Renewable Energy Laboratory, Golden CO, USA

Received: 8 May 2013 – Accepted: 29 May 2013 – Published: 19 June 2013

Correspondence to: M. J. Kleeman (mjkleeman@ucdavis.edu)

Published by Copernicus Publications on behalf of the European Geosciences Union.

Abstract

A source-oriented representation of airborne particulate matter was added to the Weather Research & Forecasting (WRF) model with chemistry (WRF/Chem). The source-oriented aerosol separately tracks primary particles with different hygroscopic properties rather than instantaneously combining them into an internal mixture. The source-oriented approach avoids artificially mixing light absorbing black + brown carbon particles with materials such as sulfate that would encourage the formation of additional coatings. Source-oriented particles undergo coagulation and gas-particle conversion, but these processes are considered in a dynamic framework that realistically "ages" primary particles over hours and days in the atmosphere. The source-oriented WRF/Chem model more accurately predicts radiative feedbacks from anthropogenic aerosols compared to models that make internal mixing or other artificial mixing assumptions.

A three-week stagnation episode (15 December 2000 to 6 January 2001) during the California Regional $PM_{10}/PM_{2.5}$Air Quality Study (CRPAQS) was chosen for the initial application of the new modeling system. Emissions were obtained from the California Air Resources Board. Gas-phase reactions were modeled with the SAPRC90 photochemical mechanism. Gas-particle conversion was modeled as a dynamic process with semi-volatile vapor pressures at the particle surface calculated using ISORROPIA. Source oriented calculations were performed for 8 particle size fractions ranging from 0.01–10 µm particle diameters with a spatial resolution of 4 km and hourly time resolution. Primary particles emitted from diesel engines, wood smoke, high sulfur fuel combustion, food cooking, and other anthropogenic sources were tracked separately throughout the simulation as they aged in the atmosphere. Results show that the source-oriented representation of particles with meteorological feedbacks in WRF/Chem changes the aerosol extinction coefficients, downward shortwave flux, and primary and secondary particulate matter concentrations relative to the internally mixed version of the model. Downward shortwave radiation predicted by source-oriented

ACPD
13, 16457–16494, 2013

model is enhanced by 1 % at ground level chiefly because diesel engine particles in the source-oriented mixture are not artificially coated with material that increases their absorption efficiency. The extinction coefficient predicted by the source-oriented WRF/Chem model is reduced by an average of ∼ 5–10 % in the central valley with a maximum reduction of ∼ 20 %. Particulate matter concentrations predicted by the source-oriented WRF/Chem model are ∼ 5–10 % lower than the internally mixed version of the same model because increased solar radiation at the ground increases atmospheric mixing. All of these results stem from the mixing state of black carbon. The source-oriented model representation with realistic aging processes predicts that hydrophobic diesel engine particles remain largely uncoated over the +7 day simulation period, while the internal mixture model representation predicts significant accumulation of secondary nitrate and water on diesel engine particles. Similar results will likely be found in any air pollution stagnation episode that is characterized by significant particulate nitrate production.

1 Introduction

The Weather Research & Forecasting (WRF) model developed primarily by the National Center for Atmospheric Research (NCAR) and the National Oceanic and Atmospheric Administration (NOAA) is frequently used to predict meteorological conditions during stagnation events that lead to high concentrations of air pollutants (Borge et al., 2008; Hu et al., 2010; Huang et al., 2010; Zhang et al., 2012). The WRF model with chemistry (WRF/Chem) allows for coupled simulations of atmospheric chemistry and meteorology so that feedbacks can be considered (Chapman et al., 2009; Grell et al., 2005). These feedback effects can be especially important during air pollution episodes that occur as a result of stagnation events. Stagnation events are characterized by weak synoptic forcing of winds, leading to the buildup of pollutant concentrations close to emissions sources. Atmospheric mixing is largely determined by the distribution of incoming radiation throughout the vertical column under these conditions. Airborne par-

ACPD
13, 16457–16494, 2013

ticles in the air pollution mixture scatter and/or absorb solar radiation which alters the vertical distribution of solar energy, atmospheric mixing, and therefore dilution rates.

The size, composition, and mixing state of airborne particles strongly affect their optical properties and therefore their effects on solar radiation (Jacobson, 2001; Mogo et al., 2012). Current versions of WRF/Chem have state-of-the-science representations of particle size and composition (Zaveri et al., 2008), but relatively simple representations of particle mixing state. WRF/Chem makes a global internal mixing assumption in which all particles with the same size in the same grid cell are instantaneously combined such that they have the same chemical composition. In reality, airborne particles become internally mixed over a period of hours to days depending on atmospheric conditions. The instantaneous internal mixing assumption alters the optical properties of particles in WRF/Chem simulations and therefore has the potential to bias air pollution – meteorology feedback calculations in the WRF/Chem model.

More sophisticated treatments of airborne particle mixing state have been used in 1-D box models (Zaveri et al., 2010) or 2-D trajectory models (Kleeman and Cass, 1998) but these frameworks cannot support a full simulation of meteorological feedbacks on a regional scale. Regional 3-D air quality models that represent particle mixing state as a source-oriented external mixture have been available for more than a decade (Held et al., 2004; Kleeman, 2001; Ying et al., 2007). These models have tracked source contributions to primary and secondary particulate matter from 8–700 sources (Hu et al., 2013; Ying et al., 2008a; Zhang et al., 2013; Zhang and Ying, 2010, 2011) but they have not attempted to calculate feedbacks to meteorology other than modification of photolysis rates (Ying and Kleeman, 2003). Basic assumptions about particle mixing state beyond the internal mixture approximation have been included in proprietary coupled meteorology-air pollution models (Jacobson, 2001). These calculations have emphasized the role of black carbon as a potential short-lived climate forcing agent, but verification of these results by the broader scientific community has not been possible due to the lack of a publically-available tool capable of such calculations.

ACPD
13, 16457–16494, 2013

The purpose of the current paper is to demonstrate how a full source-oriented representation of airborne particles would influence predicted air pollution concentrations in the publically-available WRF/Chem model. A source-oriented aerosol model represents particles emitted from different sources using separate chemical composition so that it is possible to simulate multiple particles with the same size but different chemical composition in the same grid cell. Atmospheric processes such as coagulation and gas-particle conversion age particles over time, but these processes occur over hours to days. The structure of the source-oriented WRF/Chem (SOWC) model is described, and the application of the model to a severe air pollution episode in central California is discussed. Source-oriented particles in 8 size bins are resolved for diesel engines, wood smoke, high sulfur combustion, food cooking, and other anthropogenic sources. The current study calculates from first principles the composition and mixing state of each particle source type and size bin across the domain while considering all relevant atmospheric processes including feedbacks to meteorology. Differences between model predictions for the vertical distribution of energy, momentum, and pollutant concentrations carried out with internal vs. source-oriented external representations of airborne particles are quantified, and recommendations are made for future research directions.

2 Background

Numerous air quality studies have used the source-oriented representation of particles to understand how different sources contribute to air pollution. Kleeman et al. (1997) showed that representing a plume as an externally-mixed aerosol led to specific differences in composition between particles of the same diameter. Their study showed that an externally-mixed representation will separate out species such as Na^+ and $SO_4^=$ that exist independently the real world environment, while an internally-mixed plume will combine these into one aerosol. It was also observed through their results that with increasing relative humidity, the external mixture model could accurately predict

ACPD
13, 16457–16494, 2013

a mono-disperse plume evolving into a bimodally distributed aerosol. Ying et al. (2009) studied source contributions to secondary pollutants formation within California's central valley using a source-oriented air quality model. They identified diesel engines as the largest contributor to particle nitrate and agricultural sources as the leading source of the secondary ammonium ion.

Black carbon has been identified as a major contributor to global warming (Jacobson, 1998) but the assumptions about the mixing state of black carbon (what chemical components exist in the same particles with black carbon) have a large impact on the calculation (Lesins et al., 2002; Mallet et al., 2004). Very few studies have incorporated externally mixed particles into simulations that involve radiative feedbacks, and the majority of the studies that have considered this complication have made simplifying assumptions about the mixing state of the black carbon contained in those particles. For example, Jacobson (1998) studied the effects of source-resolved aerosols on photolysis and temperatures within and above urban areas, and found that aerosols increased radiative heating within the air column, but decreased solar flux at the surface. The study assumed that when particles contained more than 5 % secondary organic material and UV wavelengths were considered, the shell was comprised of secondary organics while the rest of each particle was core material. However, when particles contained less than 5 % secondary organics and when visible wavelengths were considered, the core was assumed to be elemental (black) carbon.

California's Central Valley experiences some of the worst winter-time particulate air pollution in the United State (Ostro et al., 2006; Ostro and Chestnut, 1998; Woodruff et al., 2006) due to its unique mountain-valley topography and frequent stagnation events. The California Regional $PM_{10}/PM_{2.5}$ Air Quality Study (CRPAQS) was a field campaign starting in December 1999 and ending in January 2001. CRPAQS was designed to study the Central Valley's elevated particulate matter (PM) concentrations. During this campaign, continuous concentrations of gaseous CO, NO_X, and O_3were measured throughout the valley. In addition, four different PM sampling events lasting 3–4 days each were conducted during the winter months. These Intensive Operation

ACPD
13, 16457–16494, 2013

Periods (IOPs) collected information on particulate composition and size distributions, which can be used to support detailed modeling. Sampling and modeling studies focusing on the CRPAQS episode have been well documented (Chow et al., 2006; Ying et al., 2008b; Ying et al., 2009). The SOWC model will be applied to the CRPAQS study period in the present study.

3 Model description

This Source Oriented WRF/Chem (SOWC) model was created using the framework of the Weather Research and Forecasting model coupled with Chemistry (WRF/Chem) version 3.1.1. The changes necessary to add source-oriented aerosols to the WRF/Chem model fall within three branches of the code: the Registry, the chemistry driver, and the Eulerian-mass conservation dynamic core. Figure 1 illustrates the overall call structure of the chemistry driver, and names the files that were edited or created with the creation of the SOWC model and Fig. 2 provides the same information for code within the Eulerian mass conservation dynamic core. The details of the modification are provided in Appendix with the main features summarized below.

3.1 Representation of particles and gas-phase species

Particles in each Eulerian grid cell of the SOWC model are described by their size bin, source-origin, number concentration, and chemical composition using 6 dimension arrays ($i, k, j, source, size, species$). Number concentration and radius were included as the last two elements in the species dimension in order to simplify the coding structure. The model conserves number concentrations and mass concentration throughout the simulation of atmospheric processes including emissions, transport, deposition, coagulation, and condensation/evaporation. Particle radius is updated after each major operator step to reflect the actions of operators that differentially affect number and mass concentrations. Figure 4a illustrates a representative snapshot of source-oriented

ACPD
13, 16457–16494, 2013

particles in the current study. The gas-phase species in each grid cell are not source-oriented in the current study. Future work will extend the source-oriented treatment to gas-phase species in support of source apportionment calculations for secondary particulate matter (Ying and Kleeman, 2009; Ying et al., 2009), but these calculations have no impact on the radiative feedback between air pollution and meteorology that forms the focus of the current study.

All of the 6 dimensional arrays needed for the source-oriented particle representation were defined via the WRF registry program that was modified to accommodate arrays with dimensions higher than 4. The modified registry program in turn generates FORTRAN subroutines that accomplish i/o operations, HALO communications, and nesting communications for 6 dimensional variables. The computational burden (memory footprint, communication time, computation time) scales approximately linearly with the number of particle sources × size bins × chemical species. In order to keep computational time reasonable, a new 3 dimensional domain decomposition was specified for particle-phase variables in the $i, j, source$ dimensions. This creates a communication topology in which dedicated processors are assigned to track particles with a target source type. Communication calls between such processors are only necessary before operators that require information about all particle source types, such as radiation drivers, gas-particle conversion drivers, etc. This strategy is more efficient than using an equivalent number of processors in a 2 dimensional i, j domain decomposition because the fixed HALO region around each tile accounts for an increasingly large overhead as the tile shrinks in size.

3.2 Emissions, initial and boundary conditions

Source-oriented emissions were created in a netcdf format based on emissions inventories for the CRPAQS study period supplied by the California Air Resources Board (Ying et al., 2008a). The UCD emissions preprocessing system was used to transform regulatory inventories into source, size, and chemistry-resolved modeling inventories. As shown in Fig. 1, the process of adding fresh source-oriented emissions into the

ACPD
13, 16457–16494, 2013

SOWC model starts within the "emissions_driver" subroutine. Changes were made to map source-oriented particle-phase emissions to source-oriented particle phase state variables within SOWC.

Concentrations measured during the CRPAQS winter field campaign were used as initial and boundary conditions for SOWC calculations. These initial and boundary conditions were used extensively in previous modeling studies (Ying et al., 2008a; Ying et al., 2008b; Ying et al., 2009). In the present study, the interpolated concentrations on the western (upwind) edge of the modeling domain were averaged as a best estimate of initial aerosol concentrations. The same concentrations were specified along all four boundaries in the current study.

3.3 Gas-particle partitioning in ISORROPIA and coagulation

Gas-particle interaction is a complex process that consumes a sizeable fraction of the total chemistry-related computing time in the SOWC model. The SOWC model uses the APDC approach outlined by Jacobson (2005) for gas-particle conversion of inorganic species. In this approach, the ammonium ion is held in equilibrium while the anion concentrations are solved dynamically. Mass and charge balance equations are then used to determine final concentrations of each component. This numerical solution is stable at larger time steps (150–300 s), which greatly reduces the computational burden of gas-particle conversion. The vapor pressures of inorganic gases HNO_3, HCl, H_2SO_4, and NH_3 immediately above the particle surface are calculated using the ISORROPIA equilibrium solver. These concentrations are updated for every particle source and size bin at each model time step. Aerosol water content is calculated based on the particle composition of each particle using the ZSR method (Stokes and Robinson, 1966). The current study resolves the distribution of aerosol water among source-oriented aerosols, which may result in modified optical properties (Beaver et al., 2010) when there is a difference in chemical composition between the particles being surveyed (Fuller et al., 1999).

ACPD
13, 16457–16494, 2013

A source-oriented coagulation calculation is performed immediately following the gas-particle exchange calculations (Ying et al., 2008a; Zhang and Ying, 2010). The fastest coagulation rates occur between the smallest particles that have high Brownian diffusivity and the largest particles that provide a large target for collisions. The source-oriented algorithm transfers the mass of smaller particles involved in coagulation events to the larger particles, and reduces the number concentration of the smaller particles. The "source-origin" of the larger particles is preserved, at least approximately, since the mass added by coagulation events is generally small relative to the total mass in these size fractions.

3.4 Advection, diffusion and vertical mixing

Mass transport of the 6 dimensional source-oriented arrays is performed within the dynamic core of the WRF model. The SOWC model can only be used with the Eulerian mass-conservation dynamic core (EM_CORE) at present. The standard Runge-Kutta method is used to calculate the tendency of each scalar array variable, and then solve the corresponding ordinary differential equation in order to update the scalar value at the next time step. This operator can be separated into three steps: tendency calculations, scalar updates, and boundary condition updates.

The asymmetric convective model version 2 (ACM2) (Pleim, 2007) was added to the SOWC model to enhance the vertical mixing through a combination of non-local vertical mixing and eddy diffusion. ACM2 slightly increases the ozone transported to surface level from the upper atmosphere during winter stagnation events, which leads to improved performance for ozone and nitrate concentration predictions.

3.5 Long-wave and short-wave physics/aerosol-radiation feedback

The SOWC model uses the short-wave radiation modules developed by the Goddard Space Flight Center (GSFC). The current study introduced a comparable GSFC long-wave radiation module to the SOWC model framework (Chou and Suarez, 1999; Chou

ACPD
13, 16457–16494, 2013

et al., 2001; Chen et al., 2010). The standard WRF code used a pre-defined concentration profile of internally mixed pollutants for all aerosol optics calculations. A new subroutine was implemented within the SOWC model to calculate layer-averaged optical properties of the size and source resolved aerosols. The refractive index for each particle size and source within each layer is calculated using the volume averaging method described by Stelson (1990) applied with a core and shell model for each particle as described by Toon and Ackerman (1981). Elemental carbon and metals are assumed to reside in the particle core while semi-volatile materials and water are assumed to reside in the particle shell. A Mie routine is employed to calculate the optical properties for each particle which are combined into the grid-cell average values of single scattering albedo, asymmetry parameter, and optical thickness. These three optical parameters are then used as inputs with the standard radiation transfer code that is part of the standard WRF model.

4 Model application

The SOWC model was applied to simulate the air quality and meteorology in California's Central Valley from 15 December 2000 to 6 January 2001. The modeling domain is a pair of nested grids at 12 km × 12 km and 4 km × 4 km resolution. The coarser outer domain has 125 grid cells in each direction, while the more spatially resolved 4 km domain has 100 grid cells in the West-East direction, and 106 grid cells in the South-North direction. Both domains have 31 vertical layers to the top of the modeling-atmosphere at a pressure of 10 000 Pa. Figure 3 shows the outer and inner domains together with the surface terrain height. The outer domain encompasses the entire state of California. The inner domain extends from the San Francisco Bay Area eastward to the Sierra Nevada Mountains and then extends from the Northern Sacramento Valley area southward to the edge of the Tehachapi Mountains.

SOWC simulations were conducted without four dimensional data assimilation (FDDA) to minimize artificial forcing so that chemistry feedback effects on meteorol-

ACPD
13, 16457–16494, 2013

ogy would be most apparent. A statistical analysis shows that model meteorological errors do not increase significantly with time, but the effects of a weak upper level disturbance after 24 December 2000 are over-predicted which allows accumulated pollutant concentrations to escape from the SJV. This brief disruption undermines predicted pollutant concentrations during the latter half of the stagnation event. The analysis of pollutant concentrations in the following sections is focused on 24 December 2000, nine days into the simulation and the day before the weak upper level disturbance.

Since the purpose of this paper is to examine how the source-oriented representation of airborne particles influences feedback effects on meteorology, two sets of simulations were conducted using the same model. One run was configured as an internally mixed case, i.e. singular-source type so the source-oriented feature was concealed (internal case hereinafter). Another run was configured as a source-oriented externally mixed case, i.e. the true source-oriented run with multiple-source types (external case hereinafter). The results of the internal case and the external case are compared to see the differences caused by the source-oriented representation of particles.

5 Results and discussion

5.1 Model performance evaluation

Table 1 presents the root mean squared errors (RMSE) and mean absolute errors (MAE) of meteorological parameters predicted by external SOWC model and the internal SOWC model using all available observations within the 4 km domain illustrated in Fig. 3. The RMSE and MAE of the internal and external runs for temperature and wind speed are similar, with differences observed in RH. In contrast, the differences in concentrations of PM and gas pollutants predicted using the internal vs. source-oriented external particle representations are more pronounced. Table 2 shows the mean fractional bias (MFB) of PM and gas species predicted by the internal and external runs at 6 observation sites within the 4 km domain. The differences in secondary PM compo-

ACPD
13, 16457–16494, 2013

nents (nitrate, ammonium, and sulfate) and total $PM_{2.5}$ mass are larger than the differences in primary PM components (elemental carbon and organic carbon). The MFB of gas-phase CO, NO, and NO_2 is qualitatively similar to the performance of primary PM elemental and organic carbon, reflecting the importance of primary emissions in setting those gas phase concentrations. Ozone concentrations predicted by the internal and source-oriented external models are very similar. Previous studies have demonstrated that local production of ozone is minimal during the cold winter months in the SJV (Brown et al., 2006; Hu et al., 2010; Pun et al., 2009). The majority of the ozone measured at the surface is background ozone transported into the study domain by the significant winds at higher elevations that mixes to the surface when solar radiation warms to ground sufficiently to break the nocturnal surface inversion.

5.2 Model representation of aerosols

Figure 4 shows the calculated black carbon mixing state of the particles in the external case and the internal case at the surface in Fresno, CA at noon on 24 December 2000. In Fig. 4a, the external case version of the model predicts that black carbon is concentrated in a minor number of total airborne particles. In these particles, black carbon accounts for more than 50 % of the total mass with little hygroscopic material present. In Fig. 4b, the internal mixing model predicts that black carbon is distributed evenly across all particles in the atmosphere. This assumption artificially coats black carbon with hygroscopic material that alters the optical properties of the particles.

Figure 5 presents the mass distribution of the internal mixture particle representation as a function of particle diameter at the surface level in Fresno, CA at noon on 24 December 2000. Total particle mass has 3 modes between 0.2–0.5 µm, 2–4 µm, and > 10 µm particle diameter. Elemental carbon accounts for only a small fraction of the mass in any size bin. Primary organic carbon dominates the mass at smaller particle diameters but plays a minor role at larger particle sizes. Nitrate is the most abundant secondary component for particles with diameters between 0.15–5 µm, with additional contributions from ammonium and sulfate.

ACPD
13, 16457–16494, 2013

Figure 6 shows the mass distribution as a function of size for particles represented as a source-oriented external mixture on 24 December 2000 (9 days into the simulation). Figure 6a shows that the majority of the elemental carbon mass is concentrated in particles emitted from diesel engines. A minor amount of secondary components such as nitrate, sulfate, and ammonium only partitioned onto diesel engine particles between 0.15–0.6 µm. The majority of the diesel engine particles do not appear to undergo significant aging through accumulation of secondary coatings. Wood smoke and food cooking particles are other major sources of primary PM that do not attract large amounts of secondary coating, similar to diesel engine emissions. The majority of the secondary coating of ammonium nitrate that forms on the atmospheric aerosol is attracted to particles with hygroscopic primary emissions, such as particles emitted from the combustion of fuel with high sulfur content, and particles included in the "other sources" category in the current study. Ammonium nitrate condenses onto particles emitted from these sources with a mass mode forming between 0.2–0.6 µm that is much larger than the primary particle cores that act as the initial condensation site. Similar amounts of particulate nitrate are predicted using the source-oriented external mixture model and the internal mixture model, confirming the findings of previous studies that the primary particle mixing state does not strongly influence the saturation concentration product of gas-phase ammonia and nitric acid in the atmosphere (Kleeman and Cass, 2001; Ying et al., 2007; Ying et al., 2008a). The current study clearly demonstrates that the primary particle mixing state strongly affects the distribution of secondary ammonium nitrate on different particle cores, which in turn can strongly influence the optical properties of the atmosphere. The following sections quantify the feedback effects on meteorology and the resulting modification of pollutant concentrations based on the different treatments of particle mixing state.

5.3 Meteorological feedback effects

Figure 7 illustrates the aerosol extinction coefficients predicted by the external case and differences between external and internal cases. Figure 7a presents the 1 h averaged

ACPD
13, 16457–16494, 2013

extinction coefficient predicted by external case at noon on 24 December 2000. The highest extinction coefficients are 0.83 km^{-1} in the SJV between Fresno and Bakersfield corresponding to the location with the greatest concentration of secondary ammonium nitrate. The difference between the external and internal mixture cases (Fig. 7b) shows that extinction coefficients calculated using the internal particle representation are higher than those predicted with the source-oriented external representation in the SJV. The increased extinction is a consequence of artificially coating diesel engine particles with secondary ammonium nitrate and associated water. The differences between the external case and the internal case are as large as $-0.22\,km^{-1}$ near Bakersfield.

Downward clear-sky (aerosols but no clouds) shortwave radiation flux at the surface is the first meteorological variable affected by aerosol optical feedbacks. Figure 8a shows the downward shortwave flux predicted in the external case while Fig. 8b shows the difference in the concentrations predicted by the internal and external cases. The external case predicted as much as $5\,W\,m^{-2}$ higher short wave flux in SJV relative to the internal case ($\sim$ 1 % increase). Although this difference appears to be minor, the effects on atmospheric temperature structure, wind speed, and mixing may magnify the feedback effects on pollutant concentrations.

Figure 9 (left column) shows the temperature at 2 m above the surface (T2), wind speed in the x direction at 10 m above the surface (U10) and wind speed in the y direction at 10 m above the surface (V10) predicted by external case at noon on 24 December 2000. The right column of Fig. 9 illustrates the difference in the meteorological variables when airborne particles are represented as an internal mixture rather than a source-oriented external mixture. Predicted T2 in the SJV is $\sim$ 280 K and the maximum difference between the internal and external cases is $\sim$ 2 K. A coherent pattern of increased surface temperature in the external case is apparent in the SJV corresponding to the locations where aerosol extinction was reduced relative to the internal case. There are some points outside California where T2 in the external case was lower than T2 in the internal case. The locations over the ocean where this occurs are influenced

ACPD
13, 16457–16494, 2013

by changes in sea spray as a result of changes to wind speed. The ∼ 1 % change in T2 over the SJV does not fully characterize the magnitude of the redistribution of energy across the planetary boundary layer. Wind speeds in the SJV predicted in the external and internal cases differ by ∼ 10 % as shown in Fig. 9d and f. The external case tends to predict slightly higher U10 and lower V10 in the SJV, with implications for dilution and pollutant concentrations.

5.4 Differences in PM concentrations

The source-oriented external mixture representation for airborne particles used in this study has a more realistic representation of particle optical properties and it can also mechanistically determine the primary particle cores that attract large amounts of secondary particulate matter over the entire model domain. Figures 10–12 illustrate the source-origin of the primary particle cores that are associated with elemental carbon, nitrate and total $PM_{2.5}$. Since elemental carbon is a primary PM component, Fig. 10 illustrates a source apportionment plot. The nitrate and $PM_{2.5}$ total mass illustrated in Figs. 11 and 12 may have originated as gas-phase emissions from other sources, and so these results should not be interpreted as a regional source apportionment map. Readers are referred to the results of previous studies that performed source apportionment for all primary and secondary PM components for this information (Ying et al., 2008a; Ying et al., 2008b; Ying et al., 2009).

Figure 10 shows the predicted 24 h averaged $PM_{2.5}$ elemental carbon concentrations on 24 December 2000. Diesel engines dominate the total elemental carbon concentrations as shown in Fig. 10a. Central LA has highest elemental carbon concentration with maximum of 5.51 $\mu g\,m^{-3}$. Elemental carbon concentrations from diesel engines within the SJV are ∼ 2–3 $\mu g\,m^{-3}$ with a maximum at Bakersfield. Wood smoke contributes ∼ 0.2 $\mu g\,m^{-3}$ of elemental carbon in the SJV while high sulfur fuel combustion and food cooking are not significant contributors. Sources not resolved in the source-oriented external mixture contribute ∼ 1 $\mu g\,m^{-3}$ to elemental carbon concentrations throughout the SJV and Central LA areas. Figure 10f shows the difference in total

ACPD
13, 16457–16494, 2013

$PM_{2.5}$ elemental carbon predicted by external and internal cases. No coherent pattern can be observed in the concentration difference fields, with some localized cells experiencing a 0.07 $\mu g\,m^{-3}$ increase in elemental carbon concentrations and some cells experiencing a 0.2 $\mu g\,m^{-3}$ decrease. Elemental carbon concentrations peak during the nighttime hours during severe winter stagnation events in the SJV, making the 24 h average concentration less susceptible to changes in daytime mixing rates.

Figure 11 shows 24 h averaged $PM_{2.5}$ nitrate concentrations associated with different primary particle cores on 24 December 2000. The spatial patterns for all particle cores are similar, with high concentrations in the SJV between Fresno and Bakersfield and slightly lower concentrations in southern California (see Fig. 11a–e). On a regional basis, particles emitted from diesel engines, food cooking and combustion of high sulfur fuel have similar low amounts of particulate nitrate associated with them. The results shown in Fig. 6 illustrated that particles emitted from high sulfur fuel combustion have an affinity for nitrate formation, but these point sources are sparse on a regional scale and so high sulfur fuel combustion sources do not account for a significant amount of nitrate condensation in the SJV. Wood smoke is the most abundant explicit source of primary particles that act as a condensation site for nitrate, with a maximum associated nitrate concentration of 2.88 $\mu g\,m^{-3}$ in the SJV. It is apparent from the results shown in Fig. 11 that fresh wood smoke particles emitted in urban centers like Fresno and Bakersfield do not account for a significant fraction of these condensation sites, since the highest nitrate concentration occur to the east of these cities. Particles emitted from other sources are the dominant condensation sites for nitrate in the SJV, with maximum values as high as 11.4 $\mu g\,m^{-3}$. The differences in total $PM_{2.5}$ nitrate predicted between external and internal cases are shown in Fig. 11f. A coherent region of decreased nitrate concentrations is apparent between Fresno and Bakersfield in the SJV, with maximum concentration reductions as large as 0.77 $\mu g\,m^{-3}$. A single grid cell in the 12 km domain over the city of Barstow also experiences a large reduction in predicted nitrate concentrations under the source-oriented external treatment of particles vs. the internal treatment. It is noteworthy that nitrate concentrations increased in northern

ACPD
13, 16457–16494, 2013

California and in coastal locations by up to 0.36 $\mu g\,m^{-3}$. These differences reflect the redistribution of solar energy in the atmosphere and the subsequent feedback effects on particle concentrations.

Other primary and secondary PM components in the simulation exhibit similar behavior to either elemental carbon (primary) or nitrate (secondary) and thus are not shown. Figure 12 sums up all PM components to show total $PM_{2.5}$ mass on 24 December 2000. Contributions from primary and secondary components associated with primary diesel engine particles (Fig. 12a) have a maximum $PM_{2.5}$ concentration of $\sim$ 13.6 $\mu g\,m^{-3}$. The highest PM concentrations from diesel engines are found and around major transportation corridors. Total $PM_{2.5}$ concentrations associated with primary particles emitted from wood combustion have a maximum concentration of 46.1 $\mu g\,m^{-3}$ in the SJV between Fresno and Bakersfield, with much lower concentrations apparent in southern California. Primary particles emitted from combustion of fuel with high sulfur content also attracts secondary PM components that contribute significantly to total $PM_{2.5}$ concentrations in central California as shown in Fig. 12c. Combustion of jet fuel by two air force bases in this region accounts for the majority of these primary particle cores. Total $PM_{2.5}$ concentrations associated with primary particle cores emitted from food cooking have a maximum concentration of 6.27 $\mu g\,m^{-3}$. Primary particle cores emitted from other un-resolved sources (Fig. 12e) account for the majority of total $PM_{2.5}$ total mass because they attract large amounts of secondary ammonium nitrate condensation. Maximum $PM_{2.5}$ concentrations associated with material on these primary particle cores reaches 145 $\mu g\,m^{-3}$ in the SJV.

Figure 12f illustrates the difference in total $PM_{2.5}$ concentrations predicted using the source-oriented external mixture representation and the internal mixture representation for particles. The 24 h averaged differences in total $PM_{2.5}$ mass on 24 December 2000 ranges from -15.0 to 1.4 $\mu g\,m^{-3}$. The largest coherent patterns of differences are reductions in $PM_{2.5}$ concentrations of 3–7 % between Fresno and Bakersfield in central SJV when the source-oriented external mixture representation is employed.

ACPD
13, 16457–16494, 2013

Generally, the source-oriented external mixed representation of the particles presents a more realistic mixing scenario for elemental carbon compared to internal mixed representations or external mixing representations based on arbitrary rules. The source-oriented external case predicts that hydrophobic diesel engine particles remain largely uncoated during the 9 day simulation, while the internal mixture model predicts significant accumulation of secondary nitrate and water on diesel engine particles. The source-oriented treatment yields more accurate optical properties that provide more accurate feedbacks to meteorological conditions and pollutant concentrations. Although the changes in meteorological parameters are relative small, the effects are magnified for secondary PM concentrations, yielding significant differences in $PM_{2.5}$ total mass.

6 Conclusions

A source-oriented The Weather Research & Forecasting (WRF) model with chemistry (SOWC) was created so that airborne particulate matter with different hygroscopic and light absorption properties could be aged realistically in the atmosphere rather than instantaneously combining them into an internal mixture. The SOWC model was used to simulate a three-week winter stagnation pollution event in central California as an initial demonstration of its features. Source oriented calculations were performed for 8 particle size fractions ranging from 0.01–10 µm particle diameter with a spatial resolution of 4 km and hourly time resolution. Primary particles emitted from diesel engines, wood smoke, high sulfur combustion, food cooking, and other anthropogenic sources were tracked separately throughout the simulation as they aged in the atmosphere.

The source-oriented external mixture representation of particles and the internal mixture representation of particles with the WRF model yield different predictions for total particle mass when meteorological feedbacks are considered. The aerosol extinction coefficients, downward shortwave radiation flux, surface temperature, and wind fields all respond to the altered optical properties of the atmosphere resulting from the source-oriented external mixture representation of particles. This in turn affects the

ACPD
13, 16457–16494, 2013

predicted concentrations of primary and secondary particulate matter. All of these results stem from the mixing state of black carbon in particles within the simulation. The source-oriented model predicts that hydrophobic diesel engine particles remain largely uncoated during the simulation, while the internal mixture model predicts significant accumulation of secondary nitrate and water on diesel engine particles.

The SOWC model calculation in this study is arguably the most realistic simulation of primary particle aging over a regional scale with meteorological feedbacks enabled since it tracks particle mixing states realistically from the emissions source through the atmospheric aging calculation. The SOWC model is part of the open source WRF model and should enable useful future studies of interactions between air pollution, weather and climate. Future work should focus on including warm and cold cloud processes in the model so that climate-relevant questions can be addressed.

Supplementary material related to this article is available online at: http://www.atmos-chem-phys-discuss.net/13/16457/2013/acpd-13-16457-2013-supplement.pdf.

Acknowledgement. This study was funded by the United States Environmental Protection Agency under Grant No. R833372. Although the research described in the article has been funded by the United States Environmental Protection Agency it has not been subject to the Agency's required peer and policy review and therefore does not necessarily reflect the reviews of the Agency and no official endorsement should be inferred.

References

Beaver, M. R., Freedman, M. A., Hasenkopf, C. A., and Tolbert, M. A.: Cooling Enhancement of Aerosol Particles Due to Surfactant Precipitation, J. Phys. Chem. A, 114, 7070–7076, 2010.

ACPD
13, 16457–16494, 2013

Borge, R., Alexandrov, V., del Vas, J., Lumbreras, J., and Rodríguez, E.: A comprehensive sensitivity analysis of the WRF model for air quality applications over the Iberian Peninsula. Atmos. Environ. 42, 8560–8574, 2008.

Brown, S. G., Hyslop, N. P., Roberts, P. T., McCarthy, M. C., and Lurmann, F. W.: Wintertime vertical variations in Particulate Matter (PM) and precursor concentrations in the San Joaquin Valley during the California regional coarse PM/Fine PM Air Quality Study, J. Air Waste Manage., 56, 1267–1277, 2006.

Chapman, E. G., Gustafson Jr., W. I., Easter, R. C., Barnard, J. C., Ghan, S. J., Pekour, M. S., and Fast, J. D.: Coupling aerosol-cloud-radiative processes in the WRF-Chem model: Investigating the radiative impact of elevated point sources, Atmos. Chem. Phys., 9, 945–964, doi:10.5194/acp-9-945-2009, 2009.

Chen, S. H., Wang, S. H., and Waylonis, M.: Modification of Saharan air layer and environmental shear over the eastern Atlantic Ocean by dust-radiation effects, J. Geophys. Res.-Atmos., 115,D21202, doi:10.1029/2010JD014158, 2010.

Chow, J. C., Chen, L. W. A., Watson, J. G., Lowenthal, D. H., Magliano, K. A., Turkiewicz, K., and Lehrman, D. E.: $PM_{2.5}$ chemical composition and spatiotemporal variability during the California Regional PM_{10}/$PM_{2.5}$ Air Quality Study (CRPAQS), J. Geophys. Res.-Atmos., 111, D10S04, doi:10.1029/2005JD006457, 2006.

Fuller, K. A., Malm, W. C., and Kreidenweis, S. M.: Effects of mixing on extinction by carbonaceous particles, J. Geophys. Res.-Atmos., 104, 15941–15954, 1999.

Grell, G. A., Peckham, S. E., Schmitz, R., McKeen, S. A., Frost, G., Skamarock, W. C., and Eder, B.: Fully coupled "online" chemistry within the WRF model, Atmos. Environ., 39, 6957–6975, 2005.

Held, T., Ying, Q., Kaduwela, A., and Kleeman, M.: Modeling particulate matter in the San Joaquin Valley with a source-oriented externally mixed three-dimensional photochemical grid model, Atmos. Environ., 38, 3689–3711, 2004.

Hu, J., Ying, Q., Chen, J., Mahmud, A., Zhao, Z., Chen, S.-H., and Kleeman, M. J.: Particulate air quality model predictions using prognostic vs. diagnostic meteorology in central California, Atmos. Environ., 44, 215–226, 2010.

Hu, J., Chen, S., Wiedinmyer, C., Vandenberghe, F., Zhang, H., YIng, Q., and Kleeman, M. J.: Simulating primary $PM_{2.5}$ and $PM_{0.1}$ trace composition for epidemiological studies in California, Environ. Sci. Technol., in review, 2013.

ACPD
13, 16457–16494, 2013

Huang, M., Carmichael, G. R., Adhikary, B., Spak, S. N., Kulkarni, S., Cheng, Y. F., Wei, C., Tang, Y., Parrish, D. D., Oltmans, S. J., D'Allura, A., Kaduwela, A., Cai, C., Weinheimer, A. J., Wong, M., Pierce, R. B., Al-Saadi, J. A., Streets, D. G., and Zhang, Q.: Impacts of transported background ozone on California air quality during the ARCTAS-CARB period – a multi-scale modeling study, Atmos. Chem. Phys., 10, 6947–6968, doi:10.5194/acp-10-6947-2010, 2010.

Jacobson, M. Z.: Studying the effects of aerosols on vertical photolysis rate coefficient and temperature profiles over an urban airshed. J. Geophys. Res.-Atmos., 103, 10593–10604, 1998.

Jacobson, M. Z.: Strong radiative heating due to the mixing state of black carbon in atmospheric aerosols, Nature, 409, 695–697, 2001.

Jacobson, M. Z.: A solution to the problem of nonequilibrium acid/base gas-particle transfer at long time step, Aerosol. Sci. Tech., 39, 92–103, 2005.

Kleeman, M. J. and Cass, G. R.: Source contributions to the size and composition distribution of urban particulate air pollution, Atmos. Environ., 32, 2803–2816, 1998.

Kleeman, M. J. and Cass, G. R.: A 3D Eulerian source-oriented model for an externally mixed aerosol, Environ. Sci. Technol., 35, 4834–4848, 2001.

Kleeman, M. J., Cass, G. R., and Eldering, A.: Modeling the airborne particle complex as a source-oriented external mixture, J. Geophys. Res., 102, 21355–21372, 1997.

Lesins, G., Chylek, P., and Lohmann, U.: A study of internal and external mixing scenarios and its effect on aerosol optical properties and direct radiative forcing, J. Geophys. Res., 107, 4094, doi:10.1029/2001JD000973, 2002.

Mallet, M., Roger, J. C., Despiau, S., Putaud, J. P., and Dubovik, O.: A study of the mixing state of black carbon in urban zone, J. Geophys. Res.-Atmos., 109, D04202, doi:10.1029/2003JD003940, 2004.

Mogo, S., Cachorro, V. E., Lopez, J. F., Montilla, E., Torres, B., Rodríguez, E., Bennouna, Y., and de Frutos, A. M.: In situ measurements of aerosol optical properties and number size distributions in a coastal region of Norway during the summer of 2008, Atmos. Chem. Phys., 12, 5841–5857, doi:10.5194/acp-12-5841-2012, 2012.

Ostro, B. and Chestnut, L.: Assessing the health benefits of reducing particulate matter air pollution in the United States, Environ. Res., 76, 94–106, 1998.

Ostro, B., Broadwin, R., Green, S., Feng, W. Y., and Lipsett, M.: Fine particulate air pollution and mortality in nine California counties: results from CALFINE, Environ. Health Persp., 114, 29–33, 2006.

ACPD
13, 16457–16494, 2013

Pleim, J. E.: A combined local and nonlocal closure model for the atmospheric boundary layer. Part I: Model description and testing, J Appl. Meteorol. Clim., 46, 1383–1395, 2007.
Pun, B. K., Balmori, R. T. F., and Seigneur, C.: Modeling wintertime particulate matter formation in central California, Atmos. Environ., 43, 402–409, 2009.
Stelson, A. W.: Urban aerosol refractive index prediction by partial molar refraction approach, Environ. Sci. Technol., 24, 1676–1679, 1990.
Stokes, R. H. and Robinson, R. A.: Interactions in aqueous nonelectrolyte solutions, I. Solute-solvent equilibria, J. Phys. Chem., 70, 2126–2131, 1966.
Toon, O. B. and Ackerman, T. P.: Algorithms for the calculation of scattering by stratified spheres, Appl. Optics, 20, 3657–3660, 1981.
Woodruff, T. J., Parker, J. D., and Schoendorf, K. C.: Fine particulate matter ($PM_{2.5}$) air pollution and selected causes of postneonatal infant mortality in California, Environ. Health Persp., 114, 786–790, 2006.
Ying, Q. and Kleeman, M. J.: Effects of aerosol UV extinction on the formation of ozone and secondary particulate matter, Atmos. Environ., 37, 5047–5068, 2003.
Ying, Q. and Kleeman, M.: Regional contributions to airborne particulate matter in central California during a severe pollution episode, Atmos. Environ., 43, 1218–1228, 2009.
Ying, Q., Fraser, M. P., Griffin, R. J., Chen, J. J., and Kleeman, M. J.: Verification of a source-oriented externally mixed air quality model during a severe photochemical smog episode, Atmos. Environ., 41, 1521–1538, 2007.
Ying, Q., Lu, J., Allen, P., Livingstone, P., Kaduwela, A., and Kleeman, M. J.: Modeling air quality during the California Regional $PM_{10}/PM_{2.5}$ Air Quality Study (CRPAQS) using the UCD/CIT source-oriented air quality model – Part I. Base case model results, Atmos. Environ., 42, 8954–8966, 2008a.
Ying, Q., Lu, J., Kaduwela, A., and Kleeman, M.: Modeling air quality during the California Regional $PM_{10}/PM_{2.5}$ Air Quality Study (CPRAQS) using the UCD/CIT Source Oriented Air Quality Model – Part II. Regional source apportionment of primary airborne particulate matter, Atmos. Environ., 42, 8967–8978, 2008b.
Ying, Q., Lu, J., and Kleeman, M. J.: Modeling air quality during the California Regional $PM_{10}/PM_{2.5}$ Air Quality Study (CRPAQS) using the UCD/CIT sourceoriented air quality model – Part III. Regional source apportionment of secondary and total airborne particulate matter, Atmos. Environ., 43, 419–430, 2009.

ACPD
13, 16457–16494, 2013

Zaveri, R. A., Easter, R. C., Fast, J. D., and Peters, L. K.: Model for Simulating Aerosol Interactions and Chemistry (MOSAIC), J. Geophys. Res.-Atmos., 113, D13204, doi:10.1029/2007JD008782, 2008.

Zaveri, R. A., Barnard, J. C., Easter, R. C., Riemer, N., and West, M.: Particle-resolved simulation of aerosol size, composition, mixing state, and the associated optical and cloud condensation nuclei activation properties in an evolving urban plume, J. Geophys. Res.-Atmos., 115, D17210, doi:10.1029/2009JD013616, 2010.

Zhang, H. and Ying, Q.: Source apportionment of airborne particulate matter in Southeast Texas using a source-oriented 3D air quality model, Atmos. Environ., 44, 3547–3557, 2010.

Zhang, H. and Ying, Q.: Secondary organic aerosol formation and source apportionment in southeast Texas, Atmos. Environ., 45, 3217–3227, 2011.

Zhang, H., Li, J., Ying, Q., Yu, J. Z., Wu, D., Cheng, Y., He, K., and Jiang, J.: Source apportionment of $PM_{2.5}$ nitrate and sulfate in China using a source-oriented chemical transport model, Atmos. Environ., 62, 228–242, 2012.

Zhang, H., Li, J., Ying, Q., Guven, B. B., and Olaguer, E. P.: Source apportionment of formaldehyde during TexAQS 2006 using a source-oriented chemical transport model, J. Geophys. Res.-Atmos., 118, 1525–1535, 2013.

ACPD
13, 16457–16494, 2013

Table 1. Statistics of meteorological parameters predicted by external run and internal run for at all observation sites within 4 km domain. RMSE and MAE are the root mean squared error and the mean absolute error, respectively.

		Mean	RMSE	MAE
Temperature	Obs.	8.05		
	External	8.67	3.08	2.39
	Internal	8.67	3.09	2.39
RH	Obs.	69.94		
	External	49.99	29.57	24.69
	Internal	50.13	29.52	24.63
U wind	Obs.	1.03		
	External	1.41	1.57	1.06
	Internal	1.41	1.57	1.06
V wind	Obs.	1.08		
	External	1.51	1.81	1.19
	Internal	1.51	1.81	1.19

ACPD
13, 16457–16494, 2013

Table 2. Mean fractional biases of PM and gas species predicted by external run and internal run at 6 observation sites within 4 km domain.

SITE		ANGI	BAC	BTI	FSF	SDP	M14
$PM_{2.5}$	External	0.11	−0.67	−0.07	0.09	−0.03	–
	Internal	0.25	−0.51	−0.08	0.17	−0.04	–
N(V)	External	−0.15	−0.92	0.22	−0.69	−0.47	−0.81
	Internal	−0.11	−0.76	0.37	−0.56	−0.4	−0.62
NH_4	External	−1.34	−1.1	−0.26	−1.3	−0.5	−0.9
	Internal	−1.38	−0.94	−0.08	−1.26	−0.5	−0.76
S(VI)	External	−0.38	−0.8	0.32	0.03	−0.04	−0.36
	Internal	−0.34	−0.74	0.33	0.02	−0.04	−0.39
EC	External	0.33	−0.9	−0.04	−0.31	0.32	0.33
	Internal	0.39	−0.86	−0.08	−0.24	0.32	0.3
OC	External	−0.21	−1.01	−0.39	−0.2	−0.26	−0.54
	Internal	−0.28	−1	−0.46	−0.18	−0.64	−0.64
O_3	External	−1.19	−0.73	−0.85	−1.41	−0.33	−1
	Internal	−1.19	−0.72	−0.84	−1.41	−0.31	−1
CO	External	–	−0.34	−0.03	−0.21	−0.02	−0.29
	Internal	–	−0.3	0.03	−0.15	0.02	−0.24
NO	External	−0.04	−0.76	−0.3	−0.08	−0.56	−0.85
	Internal	0.03	−0.74	−0.25	−0.04	−0.53	−0.81
NO_2	External	0.79	−0.49	−0.49	−0.36	−0.13	−0.39
	Internal	0.82	−0.45	−0.45	−0.32	−0.1	−0.36

ACPD
13, 16457–16494, 2013

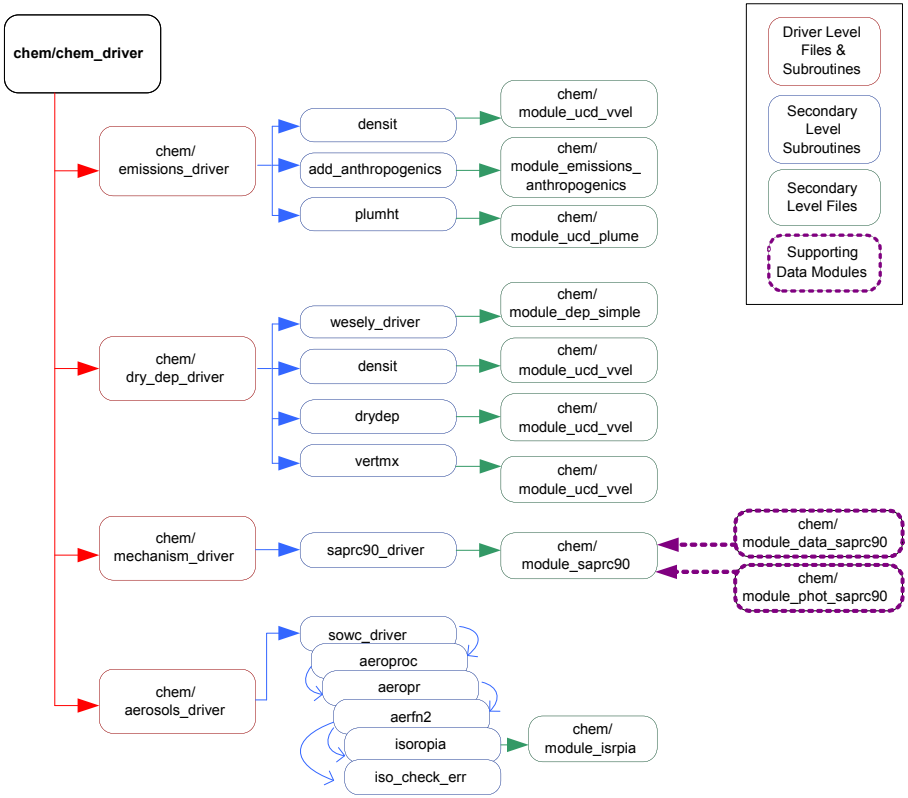

Fig. 1. Schematic showing the flow of information within the SOWC model's chemistry driver. All files, routine calls, and modules listed here were altered or newly added to the WRF framework to build the SOWC model just within the chem_driver section of the original WRF code.

ACPD
13, 16457–16494, 2013

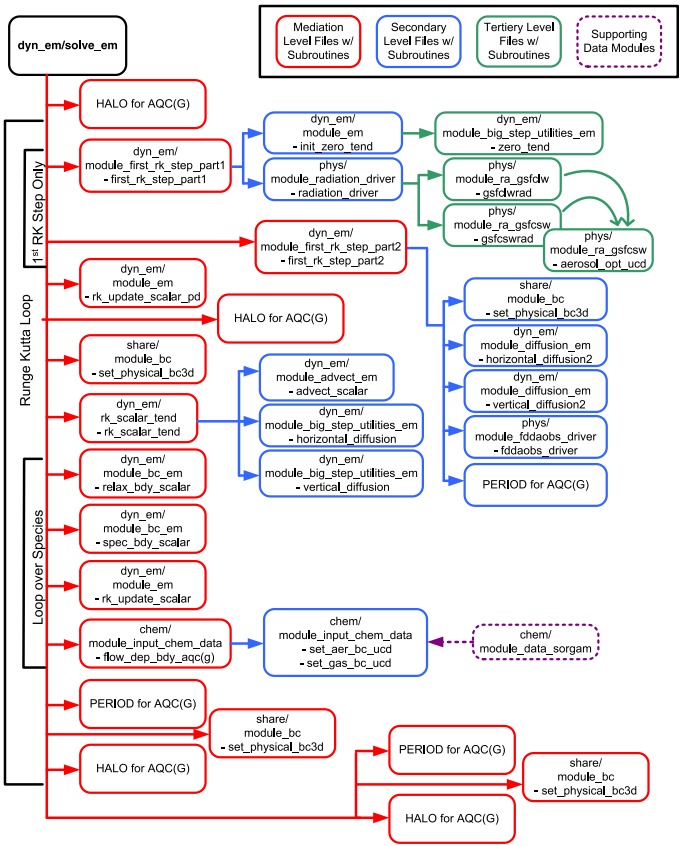

Fig. 2. Schematic showing the flow of information within the SOWC model's dynamic-Eulerian mass conservation core. All files, routine calls, and modules listed here were altered or newly added to the WRF framework to build the SOWC model just within the dynamic driver section of the original WRF code.

ACPD
13, 16457–16494, 2013

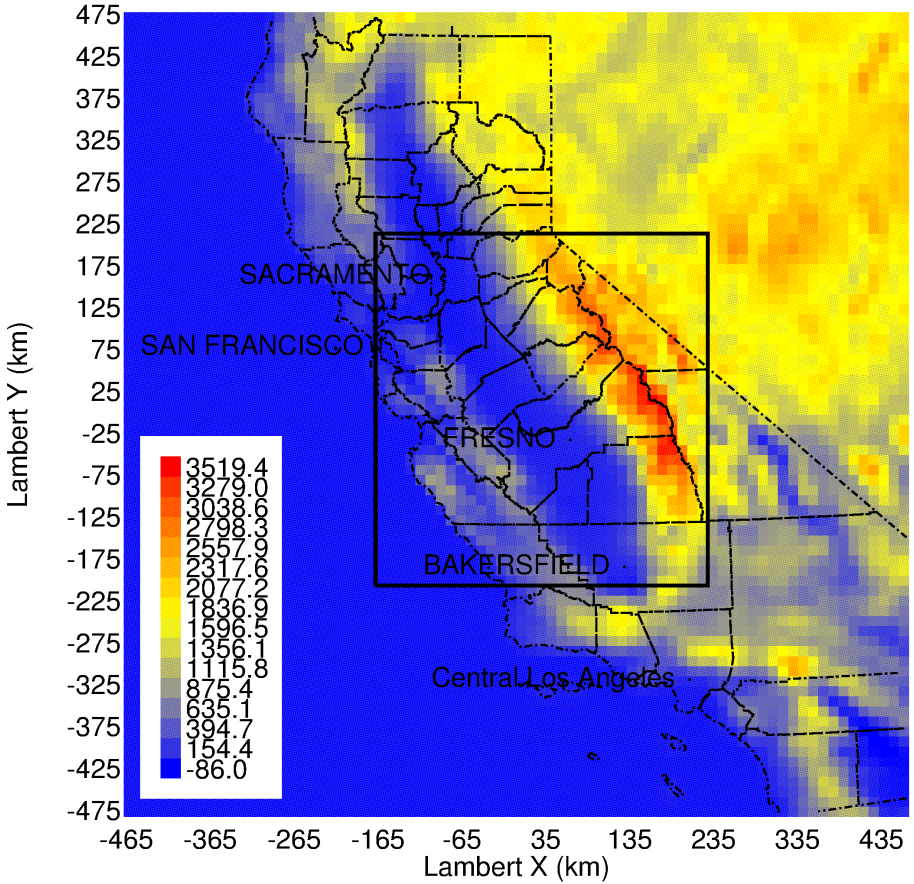

Fig. 3. Relative configuration of the nested WRF computation domains. The 4 km domain illustrated by the rectangle box covers Central Valley.

ACPD
13, 16457–16494, 2013

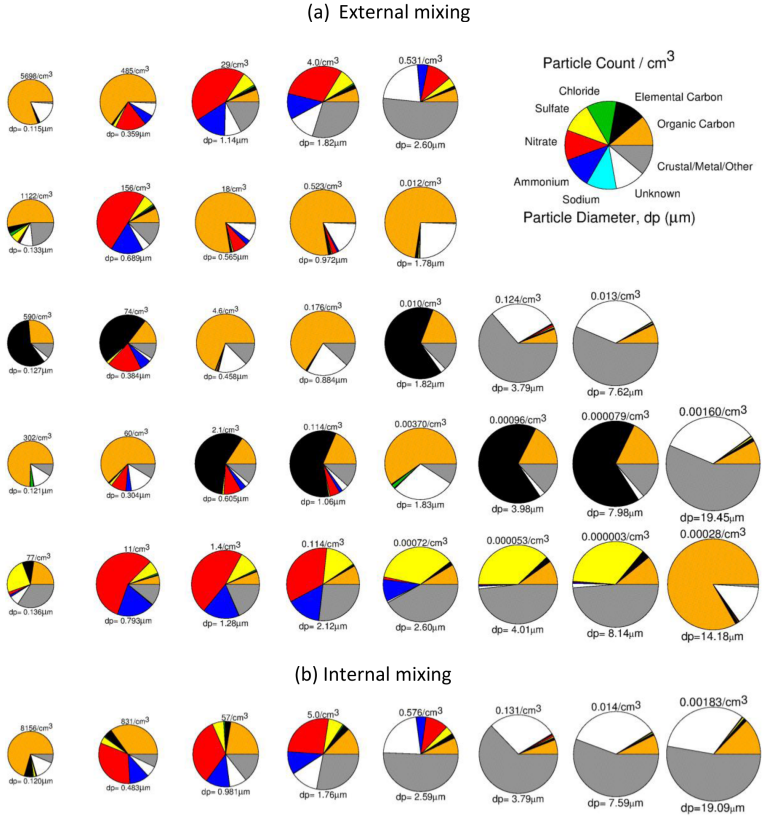

Fig. 4. (a) External and **(b)** internal mixing state of the particles at noon on 24 December 2000 at surface level in Fresno, CA. The pie charts in this figure are ordered so that the particles with the highest number concentration are at the top. All compositions in this figure represent results when the number concentration of that source and size bin is greater than $1\,m^{-3}$ (= $1.0 \times 10^{-6}\,cm^{-3}$).

ACPD
13, 16457–16494, 2013

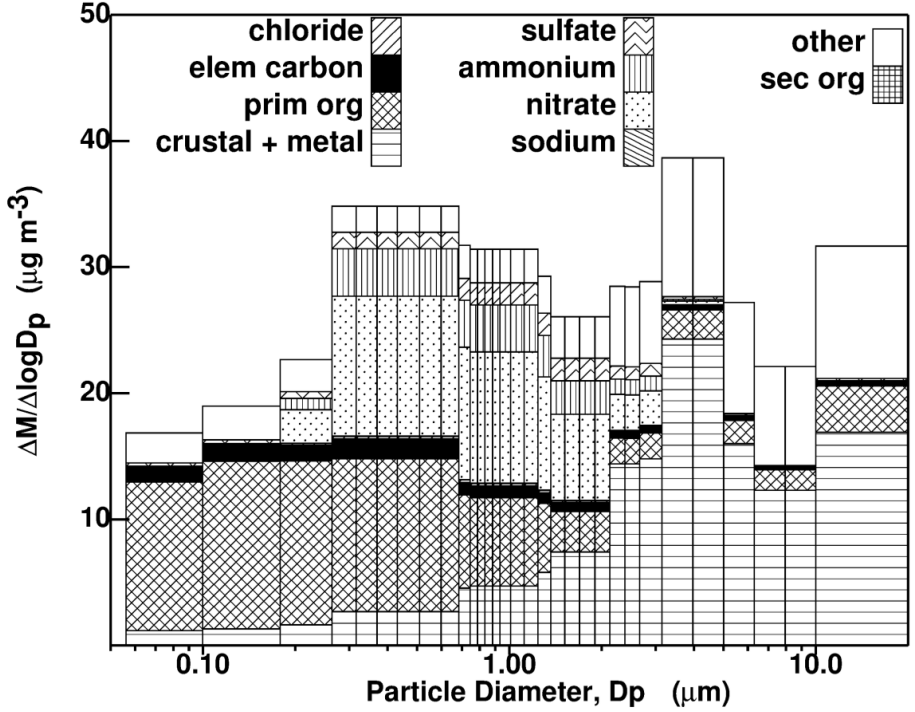

Fig. 5. Size distribution plot of the internal mixture particulate representation at Fresno, California.

ACPD
13, 16457–16494, 2013

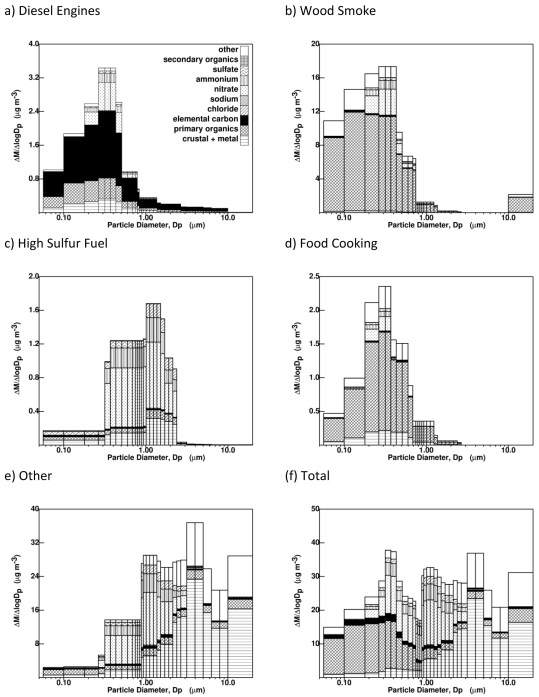

Fig. 6. Size distribiton plot of the external mixture particulate representation at Fresno, California, on 24 December 2000.

ACPD
13, 16457–16494, 2013

(a) Extinction coefficient (External case)
(noon December 24, 2000)

(b) Difference (External case – internal case)
(noon December 24, 2000)

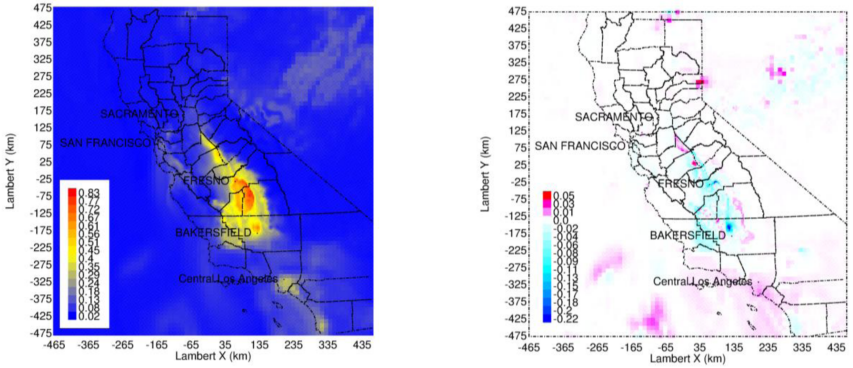

Fig. 7. (a) Calculated extinction coefficient at noon, 24 December 2000 of the external case and **(b)** difference between the external and internal case in units of km^{-1}

ACPD
13, 16457–16494, 2013

(a) Downward short wave (External case) (noon December 24, 2000)

(b) Difference (External case – Internal case) (noon December 24, 2000)

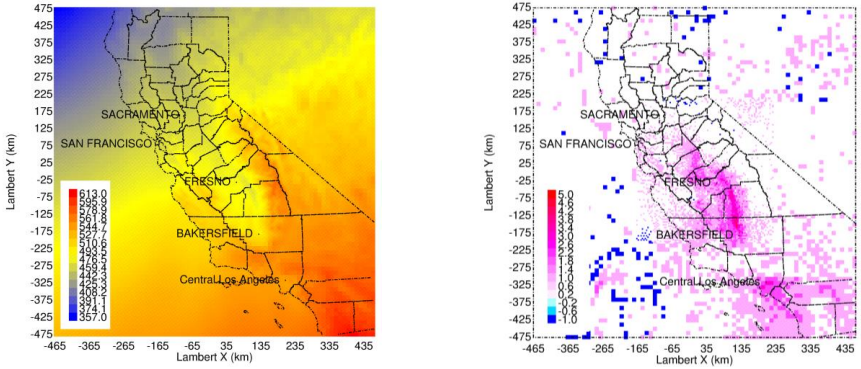

Fig. 8. Calculated clear-sky downward radiation of the **(a)** external case **(b)** difference between external case and internal case at noon, 24 December 2000 in units of W m^{-2}.

ACPD
13, 16457–16494, 2013

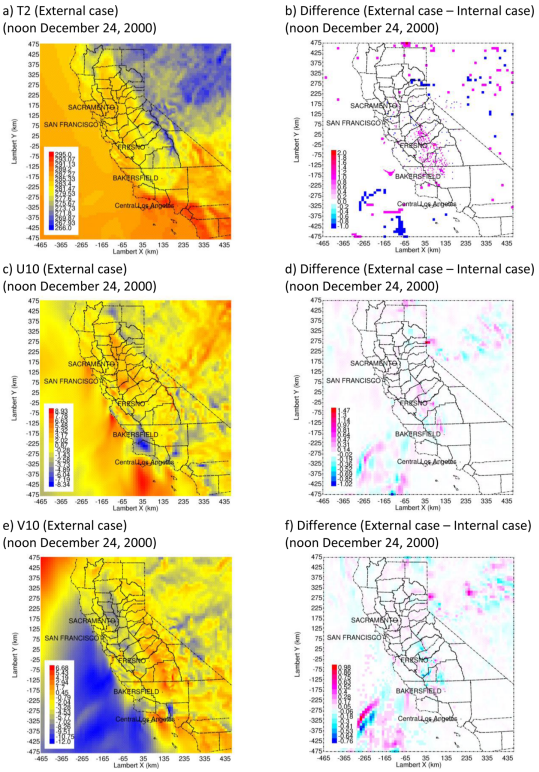

Fig. 9. Calculated T2 (K), U10 ($m\,s^{-1}$) and V10 ($m\,s^{-1}$) by external case (**a**, **c**, and **e**) at noon, 24 December 2000 and the differences between external case and internal case (**b**, **d**, and **f**).

ACPD
13, 16457–16494, 2013

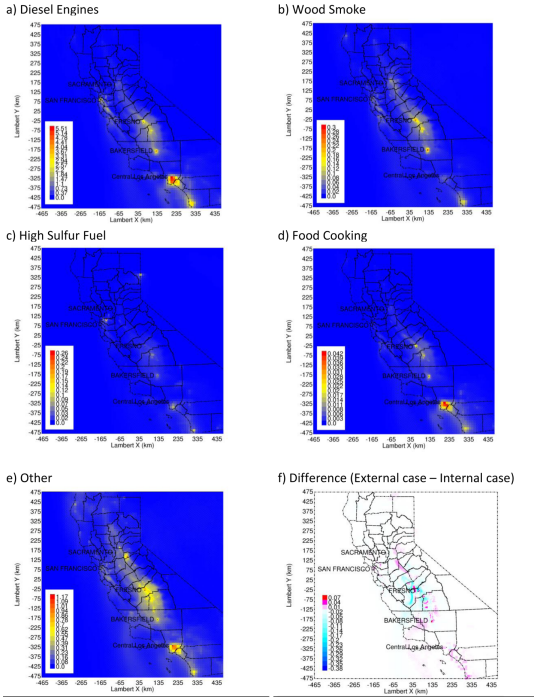

Fig. 10. 24 h averaged elemental carbon concentrations associated with primary particles emitted from different sources predicted by external case **(a–e)** on 24 December 2000 and difference between external case and internal case **(f)**. Units are $\mu g\,m^{-3}$.

ACPD
13, 16457–16494, 2013

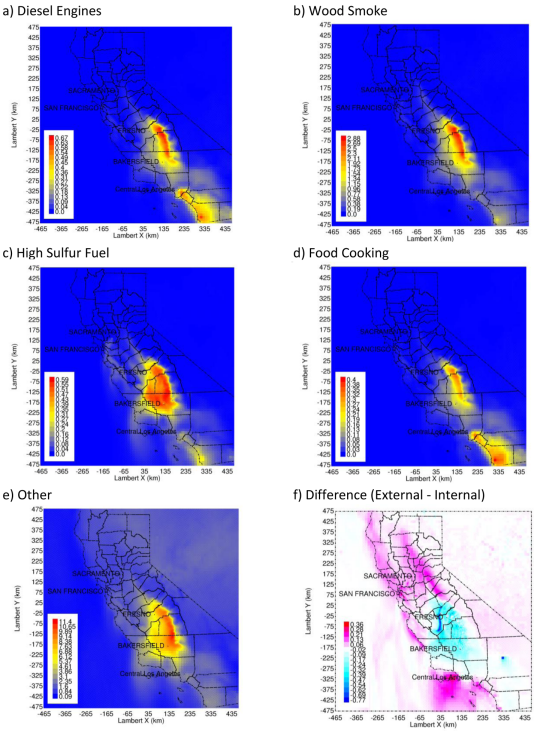

Fig. 11. 24 h averaged nitrate concentrations associated with primary particles emitted from different sources predicted by the external case **(a–e)** on 24 December 2000 and difference between external case and internal case **(f)**. Units are $\mu g\,m^{-3}$.

ACPD
13, 16457–16494, 2013

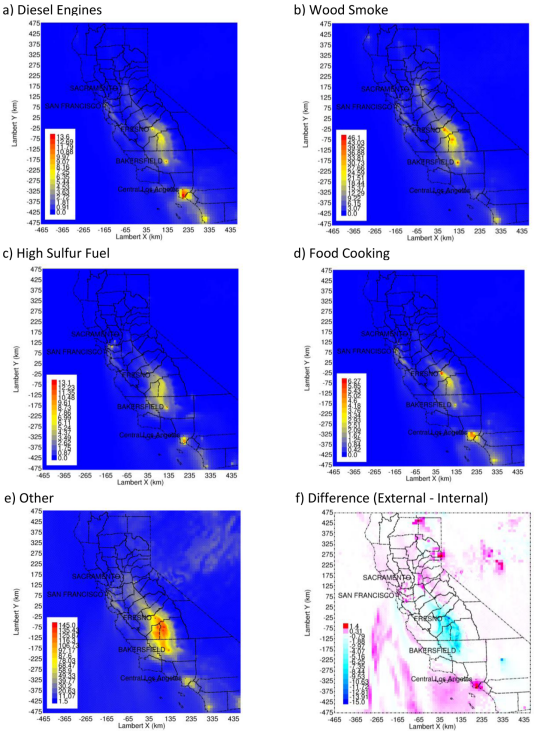

Fig. 12. 24 h averaged $PM_{2.5}$ concentrations associated with primary particles emitted from different sources predicted by the external case **(a–e)** on 24 December 2000 and difference between external case and internal case **(f)**. Units are $\mu g\,m^{-3}$.

ACPD
13, 16457–16494, 2013